Nonlinear Control of Fixed-Wing UAVs in Presence of Stochastic Winds

Jaime Rubio Hervas[a], Mahmut Reyhanoglu[b,*], Hui Tang[c], Erdal Kayacan[a]

[a] *School of Mechanical and Aerospace Engineering, Nanyang Technological University, 639798, Singapore*

[b] *Physical Sciences Department, Embry-Riddle Aeronautical University, Daytona Beach, FL 32114 USA*

[c] *Department of Mechanical Engineering, The Hong Kong Polytechnic University, Kowloon, Hong Kong*

[*] *Corresponding author: reyhanom@erau.edu*

Phone:+1-386-226 7753, Fax: +1-386-226 6621

Abstract

This paper studies the control of fixed-wing unmanned areal vehicles (UAVs) in the presence of stochastic winds. A nonlinear controller is designed based on a full nonlinear mathematical model that includes the stochastic wind effects. The air velocity is controlled exclusively using the position of the throttle, and the rest of the dynamics are controlled with the aileron, elevator, and rudder deflections. The nonlinear control design is based on a smooth approximation of a sliding mode controller. An extended Kalman filter (EKF) is proposed for the state estimation and filtering. A case study is presented: landing control of a UAV on a ship deck in the presence of wind based exclusively on LADAR measurements. The effectiveness of the nonlinear control algorithm is illustrated through a simulation example.

1. Introduction

Nonlinear control of fixed-wing UAVs has attracted considerable research efforts during recent years both for civilian and military purposes. The control approaches developed for such systems include gain scheduling, model predictive control, backstepping, sliding modes, nested saturation, fuzzy control, H_∞ control, dynamic inversion based control, model reference adaptive control, and model based fault tolerant

Nonlinear Control of Fixed-Wing UAVs in Presence of Stochastic Winds

Jaime Rubio Hervas[a], Mahmut Reyhanoglu[b,*], Hui Tang[c], Erdal Kayacan[a]

[a] *School of Mechanical and Aerospace Engineering, Nanyang Technological University, 639798, Singapore*

[b] *Physical Sciences Department, Embry-Riddle Aeronautical University, Daytona Beach, FL 32114 USA*

[c] *Department of Mechanical Engineering, The Hong Kong Polytechnic University, Kowloon, Hong Kong*

[*] *Corresponding author: reyhanom@erau.edu*

Phone:+1-386-226 7753, Fax: +1-386-226 6621

Abstract

This paper studies the control of fixed-wing unmanned areal vehicles (UAVs) in the presence of stochastic winds. A nonlinear controller is designed based on a full nonlinear mathematical model that includes the stochastic wind effects. The air velocity is controlled exclusively using the position of the throttle, and the rest of the dynamics are controlled with the aileron, elevator, and rudder deflections. The nonlinear control design is based on a smooth approximation of a sliding mode controller. An extended Kalman filter (EKF) is proposed for the state estimation and filtering. A case study is presented: landing control of a UAV on a ship deck in the presence of wind based exclusively on LADAR measurements. The effectiveness of the nonlinear control algorithm is illustrated through a simulation example.

1. Introduction

Nonlinear control of fixed-wing UAVs has attracted considerable research efforts during recent years both for civilian and military purposes. The control approaches developed for such systems include gain scheduling, model predictive control, backstepping, sliding modes, nested saturation, fuzzy control, H_∞ control, dynamic inversion based control, model reference adaptive control, and model based fault tolerant

control [1,2,4–10]. Most of these works use simplified kinematic and dynamic models ignoring the wind effects.

There are few UAV research papers that consider the wind effects in the literature. In [11], a nonlinear gust attenuation H_1 controller has been proposed to stabilize the velocity, the attitude and the angular rates. Estimation of the wind using a nonlinear disturbance observer can be found in [12]. In [13], an adaptive backstepping approach is employed to achieve directional control in presence of an unknown crosswind. Online wind parameter estimation using adaptive control techniques can be found in [14]. The work in [15] proposes an image-based visual servo control design for fixed-wing UAVs for locally tracking linear infrastructure in the presence of wind. It must be noted that only attitude and airspeed are usually controlled in the aforementioned papers, and limited attention is paid to the accurate tracking of the translational state variables.

Because of the highly nonlinear and uncertain structure of UAVs, many difficulties arise in the design of linear and nonlinear controllers. Sliding mode control is a preferable option, as it guarantees the robustness of the system against changing working conditions. In this paper, a sliding mode control strategy is proposed for the control of fixed-wing UAVs in the presence of wind. The equations of motion (EOMs) of the UAV are nonlinear, but partially affine in control input for the chosen aircraft model. It is assumed that the mean wind velocity and its direction are known constants whereas the gust has a stochastic characterization.

The main contributions of this paper are (i) the development of a novel sliding mode controller that is inherently robust to perturbations, (ii) the design of an extended Kalman filter (EKF) for state estimation purposes, and (iii) the application of the theoretical development to the autonomous landing of UAVs on moving vessels based exclusively on laser radar measurements.

This paper is organized as follows: In Section 2, a full nonlinear dynamic model of an aircraft in the presence of wind is presented. In Section 3, the development of a sliding mode controller (SMC) is described. In Section 4, an EKF method is proposed for the state estimation in the presence of noise. Section 5 gives a case study in which

the efficacy of the control algorithm is tested. Finally, some conclusions are drawn in Section 6.

2. Aircraft Dynamics

As in [16], let F_o, F_b and F_a denote the Earth-fixed frame (considered inertial under the hypothesis of flat and nonrotating Earth), the body frame, and the aerodynamic frame, respectively. The body frame F_b is defined as the aircraft-fixed axes frame (x_b, y_b, z_b), where x_b is the longitudinal axis, y_b is the lateral axis, and z_b is the directional axis. Moreover, it is assumed that x_b-z_b is the symmetry plane. In what follows, a superscript refers to the frame used within the formulations. The abbreviations $\mathrm{s}(\cdot) = \sin(\cdot)$, $\mathrm{c}(\cdot) = \cos(\cdot)$, and $\mathrm{t}(\cdot) = \tan(\cdot)$ are used throughout the paper.

An engine that can deliver a thrust T whose point of application is M, which has coordinates (x_M^b, y_M^b, z_M^b) in the body frame, is considered. It is assumed that symmetry is respected so that $y_M^b = 0$ and that the engine pitch setting is negligible.

Following [16], the translational EOMs for an aircraft having mass of m can be written as follows:

$$\dot{x}^o = V_a \mathrm{c}\gamma_{2_a} \mathrm{c}\gamma_{3_a} + V_{m_w} \mathrm{s}\psi_w + u_{g_w}^o \tag{1}$$

$$\dot{y}^o = V_a \mathrm{c}\gamma_{2_a} \mathrm{s}\gamma_{3_a} + V_{m_w} \mathrm{c}\psi_w + v_{g_w}^o \tag{2}$$

$$\dot{h}^o = V_a \mathrm{s}\gamma_{2_a} - w_{g_w}^o \tag{3}$$

$$m\dot{V}_a = -D + T\mathrm{c}\alpha_a \mathrm{c}\beta_a - mg\mathrm{s}\gamma_{2_a} - mP_1 \tag{4}$$

$$\begin{aligned} mV_a\dot{\gamma}_{3_a}\mathrm{c}\gamma_{2_a} &= Y\mathrm{c}\gamma_{1_a} + L\mathrm{s}\gamma_{1_a} - T(\mathrm{c}\alpha_a \mathrm{s}\beta_a \mathrm{c}\gamma_{1_a} - \mathrm{s}\alpha_a \mathrm{s}\gamma_{1_a}) \\ &- m(P_2\mathrm{c}\gamma_{1_a} - P_3\mathrm{s}\gamma_{1_a}) \end{aligned} \tag{5}$$

$$\begin{aligned} mV_a\dot{\gamma}_{2_a} &= -Y\mathrm{s}\gamma_{1_a} + L\mathrm{c}\gamma_{1_a} + T(\mathrm{c}\alpha_a \mathrm{s}\beta_a \mathrm{s}\gamma_{1_a} + \mathrm{s}\alpha_a \mathrm{c}\gamma_{1_a}) \\ &- W\mathrm{c}\gamma_{2_a} + m(P_2\mathrm{s}\gamma_{1_a} + P_3\mathrm{c}\gamma_{1_a}) \end{aligned} \tag{6}$$

where

$$
\begin{aligned}
P_1 &= (q_w^b w_w^b - r_w^b v_w^b)\mathrm{c}\alpha_a\mathrm{c}\beta_a + (r_w^b u_w^b - p_w^b w_w^b)\mathrm{s}\beta_a + (p_w^b v_w^b - q_w^b u_w^b)\mathrm{s}\alpha_a\mathrm{c}\beta_a \\
P_2 &= V_a(r_w^b\mathrm{c}\alpha_a - p_w^b\mathrm{s}\alpha_a) - (q_w^b w_w^b - r_w^b v_w^b)\mathrm{c}\alpha_a\mathrm{s}\beta_a + (r_w^b u_w^b - p_w^b w_w^b)\mathrm{c}\beta_a \\
&\quad - (p_w^b v_w^b - q_w^b u_w^b)\mathrm{s}\alpha_a\mathrm{s}\beta_a \\
P_3 &= V_a(p_w^b\mathrm{c}\alpha_a\mathrm{s}\beta_a - q_w^b\mathrm{c}\beta_a + r_w^b\mathrm{s}\alpha_a\mathrm{s}\beta_a) - (q_w^b w_w^b - r_w^b v_w^b)\mathrm{s}\alpha_a \\
&\quad + (p_w^b v_w^b - q_w^b u_w^b)\mathrm{c}\alpha_a
\end{aligned}
$$

Here V_a is the air speed, V_{m_w} is the mean wind speed (assumed to act in a horizontal plane at a heading angle ψ_w); $(x^o,\, y^o,\, h^o)$ denote the inertial coordinates (range, lateral displacement and altitude) of the aircraft's center of mass; $(D,\, L,\, Y)$ are the drag, lift, and side forces (see the expressions in Appendix A) which contain the aileron, elevator and rudder deflections $(\delta_a,\, \delta_e,\, \delta_r)$; g is the gravitational acceleration; $(\gamma_{1_a},\, \gamma_{2_a},\, \gamma_{3_a})$ are the aerodynamic bank angle, the aerodynamic climb angle (constrained as $\gamma_{2_a} < \pi/2$), and the aerodynamic azimuth or track angle; $(u_{g_w}^o,\, v_{g_w}^o,\, w_{g_w}^o)$ are the inertial gust velocity components; $(u_w^b,\, v_w^b,\, w_w^b)$ are the wind velocity components, and $(p_w^b,\, q_w^b,\, r_w^b)$ are the angular velocity components of the local wind in the body frame, respectively. The aerodynamic angle of attack and sideslip angle are denoted by α_a and β_a, respectively.

Again following [16], the rotational EOMs can be written as follows:

$$
\begin{bmatrix} \dot{\phi} \\ \dot{\theta} \\ \dot{\psi} \end{bmatrix} = \begin{bmatrix} 1 & \mathrm{s}\phi\mathrm{t}\theta & \mathrm{c}\phi\mathrm{t}\theta \\ 0 & \mathrm{c}\phi & -\mathrm{s}\phi \\ 0 & \frac{\mathrm{s}\phi}{\mathrm{c}\theta} & \frac{\mathrm{c}\phi}{\mathrm{c}\theta} \end{bmatrix} \begin{bmatrix} p_a^b \\ q_a^b \\ r_a^b \end{bmatrix} + \begin{bmatrix} p_w^o \frac{\mathrm{c}\psi}{\mathrm{c}\theta} + q_w^o \frac{\mathrm{s}\psi}{\mathrm{c}\theta} \\ -p_w^o\mathrm{s}\psi + q_w^o\mathrm{c}\phi \\ p_w^o\mathrm{c}\psi\mathrm{t}\theta + q_w^o\mathrm{s}\psi\mathrm{t}\theta + r_w^o \end{bmatrix} \tag{7}
$$

$$
\begin{bmatrix} \dot{p}_a^b \\ \dot{q}_a^b \\ \dot{r}_a^b \end{bmatrix} = \mathbf{I}^{-1} \begin{bmatrix} \mathcal{L} - (I_z - I_y)q_a^b r_a^b + I_{xz}p_a^b q_a^b - q_a^b h_z' + r_a^b h_y' - P_4 \\ \mathcal{M} + Tz_M^b + (I_z - I_x)p_a^b r_a^b - I_{xz}\left({p_a^b}^2 - {r_a^b}^2\right) - r_a^b h_x' + p_a^b h_z' - P_5 \\ \mathcal{N} - (I_y - I_x)p_a^b q_a^b - I_{xz}q_a^b r_a^b - p_a^b h_y' + q_a^b h_x' - P_6 \end{bmatrix} \tag{8}
$$

where

$$\mathbf{I} = \begin{bmatrix} I_x & 0 & -I_{xz} \\ 0 & I_y & 0 \\ -I_{xz} & 0 & I_z \end{bmatrix}$$

$$\begin{aligned} P_4 &= -I_{xz}(2q_a^b p_w^b + p_w^b q_w^b) + (I_z - I_y)(q_a^b r_w^b + r_a^b q_w^b + q_w^b r_w^b) \\ &\quad - I_x(q_a^b r_w^b - r_a^b q_w^b) + q_w^b h_z' - r_w^b h_y' \\ P_5 &= I_{xz}({p_w^b}^2 + 2p_a^b p_w^b - {r_w^b}^2 - 2r_a^b r_w^b) - (I_z - I_x)(p_a^b r_w^b + r_a^b p_w^b + p_w^b r_w^b) \\ &\quad - I_y(r_a^b p_w^b - p_a^b r_w^b) + r_w^b h_x' - p_w^b h_z' \\ P_6 &= I_{xz}(2q_a^b r_w^b + q_w^b r_w^b) + (I_y - I_x)(p_a^b q_w^b + q_a^b p_w^b + p_w^b q_w^b) \\ &\quad - I_z(p_a^b q_w^b - q_a^b p_w^b) + p_w^b h_y' - q_w^b h_x' \end{aligned}$$

Here $(\phi,\ \theta,\ \psi)$ denote the roll, pitch, and yaw angles; $(p_a^b,\ q_a^b,\ r_a^b)$ are the aerodynamic angular velocity vector (roll, pitch, and yaw rates) in the body frame; $(h_x',\ h_y',\ h_z')$ is the angular momentum vector of all rotors about the aircraft-fixed x_b, y_b, z_b axes; $(\mathcal{L},\ \mathcal{M},\ \mathcal{N})$ are the rolling, pitching, and yawing moments (see expressions in Appendix); $(I_x,\ I_y,\ I_z)$ are moments of inertia about the aircraft-fixed x_b, y_b, z_b axes; and I_{xz} denotes the product of inertia. Throughout the paper, 321 Euler angle sequence is used, so that $\mid \theta \mid < \pi/2$.

The angles γ_{1_a}, α_a and β_a, are defined in terms of the aerodynamic variables as follows [16]:

$$V_a = \sqrt{{u_a^b}^2 + {v_a^b}^2 + {w_a^b}^2} \tag{9}$$

$$\alpha_a = \mathrm{t}^{-1}\frac{w_a^b}{u_a^b}, \quad \beta_a = \mathrm{s}^{-1}\frac{v_a^b}{V_a} \tag{10}$$

$$\gamma_{1_a} = \mathrm{s}^{-1}\frac{\mathrm{c}\alpha_a \mathrm{s}\beta_a \mathrm{s}\theta + \mathrm{c}\beta_a \mathrm{s}\phi \mathrm{c}\theta - \mathrm{s}\alpha_a \mathrm{s}\beta_a \mathrm{c}\phi \mathrm{c}\theta}{\mathrm{c}\gamma_{2_a}} \tag{11}$$

in the formulation above, where $(u_a^b,\ v_a^b,\ w_a^b)$ are the air velocity components in the body frame. It should be noted that

$$\gamma_{1_a} = \mathrm{c}^{-1}\frac{\mathrm{s}\alpha_a \mathrm{s}\theta + \mathrm{c}\alpha_a \mathrm{c}\phi \mathrm{c}\theta}{\mathrm{c}\gamma_{2_a}} \tag{12}$$

A simple model is generally used to define the modulus of thrust for a propeller propulsion engine as follows:

$$T = \frac{k_m \rho}{V_a} \eta \tag{13}$$

where k_m is a constant and η represents the position of the throttle (between 0 and 1 inclusive).

Defining the state and control vectors as $\hat{\boldsymbol{\xi}} = [x^o,\, y^o,\, h^o,\, V_a,\, \gamma_{2_a},\, \gamma_{3_a},\, \phi,\, \theta,\, \psi,\, p_a^b,\, q_a^b,\, r_a^b]^T$ and $\hat{\mathbf{u}} = [\eta,\, \delta_a,\, \delta_e,\, \delta_r]$, respectively; and treating the stochastic terms coming from the gusts $\boldsymbol{\sigma} = [u_{g_w}^o,\, v_{g_w}^o,\, w_{g_w}^o,\, p_w^o,\, q_w^o,\, r_w^o]^T$ as perturbations $\mathbf{p}(\hat{\boldsymbol{\xi}},\, \boldsymbol{\sigma})$, the aircraft dynamics can be expressed as follows:

$$\dot{\hat{\boldsymbol{\xi}}} = \hat{\mathbf{f}}(\hat{\boldsymbol{\xi}}) + \hat{\mathbf{g}}(\hat{\boldsymbol{\xi}},\, \hat{\mathbf{u}}) + \mathbf{p}(\hat{\boldsymbol{\xi}},\, \boldsymbol{\sigma}) \tag{14}$$

3. Control Algorithm

The control design is formulated into a trajectory tracking problem. For simplicity, it is assumed that the mean wind velocity and its direction are known constants whereas the gust has a stochastic characterization.

Equation (4) for the air velocity dynamics can be rewritten as

$$\dot{V}_a = \frac{-D + T\mathrm{c}\alpha_a \mathrm{c}\beta_a}{m} - g\mathrm{s}\gamma_{2_a} - P_1 \tag{15}$$

where the thrust T is given by (13). Therefore, assuming that the state $\hat{\boldsymbol{\xi}}$ is measurable and taking η as the control input, the air velocity equation can be expressed as

$$\dot{V}_a = -\frac{D(\hat{\boldsymbol{\xi}})}{m} + \left(\frac{k_m \rho}{m V_a} \mathrm{c}\alpha_a \mathrm{c}\beta_a\right) \eta - g\mathrm{s}\gamma_{2_a} - P_1 \tag{16}$$

Denote by V_{a_d} the reference velocity and define the velocity error as $e_{V_a} := V_a - V_{a_d}$. Then, the velocity error dynamics are given by

$$\dot{e}_{V_a} = -\frac{D(e_{V_a} + V_{a_d},\, \hat{\boldsymbol{\xi}})}{m} + \left[\frac{k_m \rho}{m\,(e_{V_a} + V_{a_d})} \mathrm{c}\alpha_a \mathrm{c}\beta_a\right] \eta - g\mathrm{s}\gamma_{2_a} - P_1 - \dot{V}_{a_d} \tag{17}$$

Proposition 1: *Consider the system* (17)*. The feedback control law given by*

$$\eta = \frac{e_{V_a} + V_{a_d}}{k_m \rho} \frac{m}{\mathrm{c}\alpha_a \mathrm{c}\beta_a} \left[g\mathrm{s}\gamma_{2_a} + \dot{V}_{a_d} + \frac{D(e_{V_a} + V_{a_d},\, \hat{\boldsymbol{\xi}})}{m} - k_{V_a} \mathrm{sign}(e_{V_a})\right] \tag{18}$$

where

$$k_{V_a} > \max |P_1| > 0 \tag{19}$$

guarantees convergence of e_{V_a} *to zero.*

Proof: Choose a candidate Lyapunov function:

$$E = \frac{1}{2} e_{V_a}^2 \tag{20}$$

such that the time derivative of E along the trajectories of (17) with feedback control input (18) is given by:

$$\dot{E} = -e_{V_a} \left(P_1 + k_{V_a} \text{sign}(e_{V_a}) \right) \tag{21}$$

which is negative definite under the condition (19) and, thus, e_{V_a} will decay to zero. ■

Remark 1: *In this paper, the signum function is defined as*

$$\text{sign(s)} = \begin{cases} 1 & \text{if} \quad s > 0 \\ 0 & \text{if} \quad s = 0 \\ -1 & \text{if} \quad s < 0 \end{cases}$$

In the literature, the sign function is undefined at 0, or it is defined as a point set mapping, i.e., $sign(0) \in [-1, 1]$. *In this paper, we define it as* $\text{sign}(0) = 0$.

In our simulations to alleviate the chattering and speed up the simulations, the following smooth approximation of the discontinuous signum function is used:

$$\text{sign}(s) \approx \tanh(ks) \tag{22}$$

where k *is a sufficiently large positive constant. Stability properties of the system (17) with the smooth implementation of the control law (18) can be analyzed using the ideas in [3]. In particular, it can be shown that the system converges to a small neighborhood of the origin. That is, the closed-loop system can be shown to be globally uniformly ultimately bounded with respect to a compact set around the origin. This set can be made arbitrarily small by increasing the slope* k *of the* $\tanh(ks)$ *function at* $s = 0$.

A sliding mode controller (SMC) is now introduced to control the rest of the dynamics. Since the control law (18) has been already introduced for the throttle,

only 3 active control inputs ($\delta_a,\ \delta_e$, and δ_r) are available. Therefore, the reduced state equations (14) with state and control input vectors given by

$$\boldsymbol{\xi} = [y^o,\, h^o,\, \gamma_{2_a},\, \gamma_{3_a},\, \phi,\, \theta,\, \psi,\, p_a^b,\, q_a^b,\, r_a^b]^T,\ \mathbf{u} = [\delta_a,\, \delta_e,\, \delta_r]^T$$

can be rewritten as

$$\dot{\boldsymbol{\xi}} = \mathbf{f}(\boldsymbol{\xi}) + \mathbf{g}(\boldsymbol{\xi},\, \mathbf{u}) + \mathbf{p}(\boldsymbol{\xi}, \boldsymbol{\sigma}) \tag{23}$$

Note that the range x^o (which is closely related to the air velocity) is not included in the above formulation. Partition the state as $\boldsymbol{\xi} = [\boldsymbol{\xi}_1^T,\, \boldsymbol{\xi}_2^T]^T$, where

$$\boldsymbol{\xi}_1 = [y^o,\, h^o,\, \gamma_{2_a},\, \gamma_{3_a},\, \phi,\, \theta,\, \psi]^T, \quad \boldsymbol{\xi}_2 = [p_a^b,\, q_a^b,\, r_a^b]^T \tag{24}$$

so that the state equations can be rewritten as

$$\dot{\boldsymbol{\xi}}_1 = \mathbf{f}_1(\boldsymbol{\xi}) + \mathbf{g}_1(\boldsymbol{\xi},\, \mathbf{u}) + \mathbf{p}_1(\boldsymbol{\xi}, \boldsymbol{\sigma}) \tag{25}$$

$$\dot{\boldsymbol{\xi}}_2 = \mathbf{f}_2(\boldsymbol{\xi}) + \mathbf{g}_2(\boldsymbol{\xi})\mathbf{u} + \mathbf{p}_2(\boldsymbol{\xi}, \boldsymbol{\sigma}) \tag{26}$$

Without loss of generality, assume that the desired (reference) trajectory is given by $y_d^o = h_d^o = 0$, where a subscript d denotes the desired variable. Consider the following transformation:

$$\begin{bmatrix} \phi_d \\ \theta_d \\ \psi_d \end{bmatrix} = \begin{bmatrix} 0 \\ \alpha_0 + \gamma_{2_{a\,d}} \\ \gamma_{3_{a\,d}} \end{bmatrix} \tag{27}$$

where α_0 denotes the trim angle of attack (assumed to be known). Based on equations (2) and (3), $\gamma_{2_{a\,d}}$ and $\gamma_{3_{a\,d}}$ can be chosen as

$$\gamma_{2_{a\,d}} = -\mathrm{s}^{-1}\left(k_{\gamma_{2_a}} \mathrm{sign}(h^o)\right) \tag{28}$$

$$\gamma_{3_{a\,d}} = -\mathrm{s}^{-1}\left(k_{\gamma_{3_a}} \mathrm{sign}(y^o) + \frac{V_{m_w} \mathrm{c}\psi_w}{V_a \mathrm{c}\gamma_{2_a}}\right) \tag{29}$$

where

$$1 > k_{\gamma_{2_a}} > \max\left|\frac{w_{g_w}^o}{V_a}\right| > 0 \tag{30}$$

$$1 - \left|\frac{V_{m_w} \mathrm{c}\psi_w}{V_a \mathrm{c}\gamma_{2_a}}\right| > k_{\gamma_{3_a}} > \max\left|\frac{v_{g_w}^o}{V_a \mathrm{c}\gamma_{2_a}}\right| > 0 \tag{31}$$

For simplicity, it will be assumed that $V_a \mathrm{c}\gamma_{2_a} \approx V_d$ in (29). This assumption can be easily relaxed.

Proposition 2: *Define the sliding functions as*

$$\mathbf{s} = \begin{bmatrix} \lambda_{\dot{\phi}} \left(\dot{\phi} - \dot{\phi}_d \right) + \lambda_{\phi} \left(\phi - \phi_d \right) \\ \lambda_{\dot{\theta}} \left(\dot{\theta} - \dot{\theta}_d \right) + \lambda_{\theta} \left(\theta - \theta_d \right) \\ \lambda_{\dot{\psi}} \left(\dot{\psi} - \dot{\psi}_d \right) + \lambda_{\psi} \left(\psi - \psi_d \right) \end{bmatrix} \tag{32}$$

where λ_{ϕ}, λ_{θ}, λ_{ψ}, $\lambda_{\dot{\phi}}$, $\lambda_{\dot{\theta}}$, and $\lambda_{\dot{\psi}}$ are positive constants. Assume that the following condition holds

$$C_{l_{\delta_a}} C_{n_{\delta_r}} \neq C_{n_{\delta_a}} C_{l_{\delta_r}} \tag{33}$$

Then, the matrix $\frac{\partial \mathbf{s}}{\partial \boldsymbol{\xi}_2} \mathbf{g}_2(\boldsymbol{\xi})$ is non-singular.

Proof: It can be easily shown that

$$\frac{\partial \mathbf{s}}{\partial \boldsymbol{\xi}_2} \mathbf{g}_2(\boldsymbol{\xi}) = QS \begin{bmatrix} \lambda_{\dot{\phi}} & \lambda_{\dot{\phi}} \mathrm{s}\phi \mathrm{t}\theta & \lambda_{\dot{\phi}} \mathrm{c}\phi \mathrm{t}\theta \\ 0 & \lambda_{\dot{\theta}} \mathrm{c}\phi & -\lambda_{\dot{\theta}} \mathrm{s}\phi \\ 0 & \lambda_{\dot{\psi}} \frac{\mathrm{s}\phi}{\mathrm{c}\theta} & \lambda_{\dot{\psi}} \frac{\mathrm{c}\phi}{\mathrm{c}\theta} \end{bmatrix} \hat{\mathbf{I}} \tag{34}$$

where

$$\hat{\mathbf{I}} = \begin{bmatrix} b \frac{I_z C_{l_{\delta_a}} + I_{xz} C_{n_{\delta_a}}}{I_x I_z - I_{xz}^2} & 0 & b \frac{I_z C_{l_{\delta_r}} + I_{xz} C_{n_{\delta_r}}}{I_x I_z - I_{xz}^2} \\ 0 & c \frac{C_{m_{\delta_e}}}{I_y} & 0 \\ b \frac{I_{xz} C_{l_{\delta_a}} + I_x C_{n_{\delta_a}}}{I_x I_z - I_{xz}^2} & 0 & b \frac{I_{xz} C_{l_{\delta_r}} + I_x C_{n_{\delta_r}}}{I_x I_z - I_{xz}^2} \end{bmatrix} \tag{35}$$

which is clearly invertible if the condition (33) holds. ■

Proposition 3: *Consider the system* (23) *with the control law*

$$\mathbf{u} = - \left(\frac{\partial \mathbf{s}}{\partial \boldsymbol{\xi}_2} \mathbf{g}_2(\boldsymbol{\xi}) \right)^{-1} \left[\frac{\partial \mathbf{s}}{\partial \boldsymbol{\xi}} \mathbf{f}(\boldsymbol{\xi}) + \mathbf{L} \operatorname{sign}(\mathbf{s}) \right] \tag{36}$$

where $\mathbf{L} = \operatorname{diag}\{L_i\}$, $i = 1, 2, 3$, such that $L_i > \left| \frac{\partial \mathbf{s}}{\partial \boldsymbol{\xi}} \mathbf{p} \right|_i$, $\forall t$. Then the system trajectory converges to the desired trajectory $y_d^0 = h_d^0 = 0$.

Proof : Define the following positive definite Lyapunov function in terms of the sliding functions (32):

$$E = \frac{1}{2} \mathbf{s}^T \mathbf{s} \tag{37}$$

Taking its time derivative yields

$$\dot{E} = \mathbf{s}^T \dot{\mathbf{s}} = \mathbf{s}^T \frac{\partial \mathbf{s}}{\partial \boldsymbol{\xi}} \dot{\boldsymbol{\xi}} = \mathbf{s}^T \frac{\partial \mathbf{s}}{\partial \boldsymbol{\xi}} \left[\mathbf{f}(\boldsymbol{\xi}) + \mathbf{g}(\boldsymbol{\xi},\, \mathbf{u}) + \mathbf{p}(\boldsymbol{\xi}, \boldsymbol{\sigma}) \right] \tag{38}$$

It can be easily shown that the sliding functions given by (32) satisfy

$$\frac{\partial \mathbf{s}}{\partial \boldsymbol{\xi}} \mathbf{g}(\boldsymbol{\xi},\, \mathbf{u}) = \frac{\partial \mathbf{s}}{\partial \boldsymbol{\xi}_2} \mathbf{g}_2(\boldsymbol{\xi}) \mathbf{u} \tag{39}$$

and therefore (38) can be rewritten as

$$\dot{E} = \mathbf{s}^T \left[\frac{\partial \mathbf{s}}{\partial \boldsymbol{\xi}} \left[\mathbf{f}(\boldsymbol{\xi}) + \mathbf{p}(\boldsymbol{\xi}, \boldsymbol{\sigma}) \right] + \frac{\partial \mathbf{s}}{\partial \boldsymbol{\xi}_2} \mathbf{g}_2(\boldsymbol{\xi}) \mathbf{u} \right] \tag{40}$$

Clearly, the control law (36) yields

$$\dot{E} = \mathbf{s}^T \left(\frac{\partial \mathbf{s}}{\partial \boldsymbol{\xi}} \mathbf{p} - \mathbf{L}\, \mathrm{sign}(\mathbf{s}) \right) \tag{41}$$

which is negative definite if the matrix $\mathbf{L}$ satisfies the conditions of the proposition. This guarantees convergence of the roll, pitch and yaw angles to their desired values given by (27). As shown in Remark 2, this implies that γ_{2_a} and γ_{3_a} will converge to their desired values $\gamma_{2_{a\,d}}$ and $\gamma_{3_{a\,d}}$, respectively; which by definitions (28)-(29) together with equations (2)-(3) implies the following

$$\dot{y}^o = -V_a \mathrm{c}\gamma_{2_a} k_{\gamma_{3_a}} \mathrm{sign}(y^o) + v^o_{g_w} \tag{42}$$

$$\dot{h}^o = -V_a k_{\gamma_{2_a}} \mathrm{sign}(h^o) - w^o_{g_w} \tag{43}$$

A similar Lyapunov approach can be used as above together with conditions (30)-(31) to subsequently ensure convergence of the inertial coordinates y^o and h^o to their desired values (i.e., the origin). ■

Remark 2: *Assume that the Euler angles ϕ, θ and ψ converge to their desired values so that*

$$\begin{bmatrix} \phi \\ \theta \\ \psi \end{bmatrix} = \begin{bmatrix} 0 \\ \alpha_0 + \gamma_{2_{a\,d}} \\ \gamma_{3_{a\,d}} \end{bmatrix} \tag{44}$$

Using equations (10)-(12)*, it can be shown that*

$$\mathrm{s}\beta_a = \mathrm{c}\gamma_{2_a}\mathrm{s}(\gamma_{3_a} - \gamma_{3_{ad}}) \tag{45}$$

$$\mathrm{t}\alpha_a = \frac{\mathrm{c}\gamma_{2_a}\mathrm{s}(\alpha_0 + \gamma_{2_{ad}})\mathrm{c}(\gamma_{3_a} - \gamma_{3_{ad}}) - \mathrm{s}\gamma_{2_a}\mathrm{c}(\alpha_0 + \gamma_{2_{ad}})}{\mathrm{c}\gamma_{2_a}\mathrm{c}(\alpha_0 + \gamma_{2_{ad}})\mathrm{c}(\gamma_{3_a} - \gamma_{3_{ad}}) + \mathrm{s}\gamma_{2_a}\mathrm{s}(\alpha_0 + \gamma_{2_{ad}})} \tag{46}$$

$$\mathrm{s}\gamma_{1_a} = \mathrm{s}\beta_a \frac{\mathrm{s}(\alpha_0 + \gamma_{2_{ad}} - \alpha_a)}{\mathrm{c}\gamma_{2_a}} \tag{47}$$

$$\mathrm{c}\gamma_{1_a} = \frac{\mathrm{c}(\alpha_0 + \gamma_{2_{ad}} - \alpha_a)}{\mathrm{c}\gamma_{2_a}} \tag{48}$$

which yields

$$\alpha_a = \alpha_0,\ \gamma_{2_a} = \gamma_{2_{ad}},\ \gamma_{3_a} = \gamma_{3_{ad}}$$

It must be noted that the computed control inputs are subject to saturation and rate limits. In particular, the maximum computed control inputs are given by:

$$\mathbf{u}_{\max} = \left(\frac{\partial \mathbf{s}}{\partial \boldsymbol{\xi}_2}\mathbf{g}_2(\boldsymbol{\xi})\right)^{-1}\mathbf{L}$$

where gains can be appropriately changed to achieve a satisfactory performance. Again, to smoothen the control inputs, the smooth approximation (22) of the signum function can be used. Given the introduction of the matrix $\mathbf{L}$ in the controller, the design is robust and estimation errors are acceptable for the stability derivatives. In this regard, a minimum amount of information is needed to implement the controller.

4. Noise Addition and Filtering

Define the random variable $\mathbf{w}$ representing the process noise so that (14) can be written as

$$\dot{\hat{\boldsymbol{\xi}}} = \hat{\mathbf{f}}(\hat{\boldsymbol{\xi}}) + \hat{\mathbf{g}}(\hat{\boldsymbol{\xi}},\ \hat{\mathbf{u}}) + \mathbf{w} \tag{49}$$

Given an output vector $\boldsymbol{\eta}$ and measurement noise vector $\mathbf{v}$, the observation equation can be expressed as

$$\boldsymbol{\eta} = \mathbf{h}(\hat{\boldsymbol{\xi}}) + \mathbf{v} \tag{50}$$

Equations (49) together with (50) describe the system required for the EKF implementation. In this paper it is assumed that $\mathbf{w}$ and $\mathbf{v}$ are zero-mean gaussian white noises with covariance matrices $\mathbf{Q}$ and $\mathbf{R}$, respectively.

5. Case Study: Autonomous Landing via a LADAR System

In this section, the theoretical development is applied to autonomous landing of a UAV on a moving vessel. As in [17], it is assumed that a LADAR system mounted on the vessel is exclusively available for the estimation of the UAV's inertial position and attitude.

5.1. LADAR Observation Model

LADAR technology consists of a modulated laser emitter coupled with a focal plane array detector and the required optics. This sensor creates an "image" of the environment, but producing a 2D image where each pixel has an associated range and intensity value. A typical algorithm first converts the imaging sensor measurements to a 3D point cloud, and then significant environmental features such as planar, line or point features are extracted from one 3D imaging sensor frame to the next. Finally, characteristics of those features such as the direction vectors are used to compute the platform position and attitude changes. In this paper, it will be assumed that a set of N points Q_i $(i = 1, \ldots, N)$ are identified by the LADAR at every time step (given by its sampling rate) based on their reflectance characteristics and that those points can be identified from one frame to the next.

Let us denote by $\mathbf{r}_{iL}$ and $\mathbf{r}_{O_bL}$ the position vectors of a point Q_i on the aircraft and the origin of the aircraft body frame O_b with respect to the LADAR, respectively; and $\mathbf{r}_{iO_b}$ the position vector from O_b to Q_i (see Fig. 1). Then, the following equations can be written:

$$\mathbf{r}^s_{O_bL} + \mathbf{T}_{sb}\mathbf{r}^b_{iO_b} = \mathbf{r}^s_{iL}, \quad \forall i \tag{51}$$

where $\mathbf{T}_{sb}$ represents the rotation matrix from the UAV-fixed body frame to the LADAR frame. Note that the vectors $\mathbf{r}^s_{iL}$ and $\mathbf{r}^b_{iO_b}$ are known from the LADAR observations and the geometry of the aircraft is assumed to be known; however, $\mathbf{r}^s_{O_bL}$ is not known a priori.

Using equation (51), the following can be obtained:

$$\mathbf{T}_{sb}\mathbf{a}^b_{ij} = \mathbf{b}^s_{ij}, \quad \forall i, j, \quad i \neq j \tag{52}$$

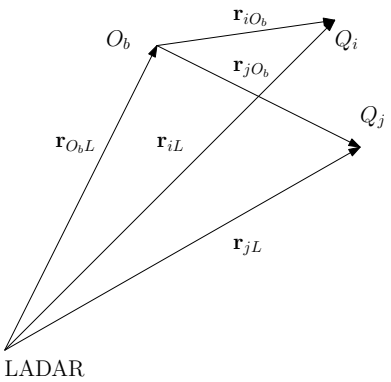

Figure 1: Relations between points on the aircraft and their LADAR observations.

where $\mathbf{a}_{ij}^b = \mathbf{r}_{iO_b}^b - \mathbf{r}_{jO_b}^b$ and $\mathbf{b}_{ij}^s = \mathbf{r}_{iL}^s - \mathbf{r}_{jL}^s$.

Since usually $M > 2$ observations are available, a statistical method can be applied to make use of all the information. One way to state the problem is to find a matrix $\mathbf{T}_{sb}$ that minimizes the loss function J defined as:

$$J(\mathbf{T}_{sb}) = \frac{1}{2}\sum_{l=1}^{M} w_l \mid \mathbf{b}_l^s - \mathbf{T}_{sb}\mathbf{a}_l^b \mid^2 \tag{53}$$

where w_l denote the weightings. Different methods are available in the literature to solve this minimization problem. In this paper, an exact method known as the "q-method" [18] is chosen. The details of this method can be found in [18].

Once the relative orientation matrix $\mathbf{T}_{sb}$ is estimated, equation (51) can be used to determine the position of the origin of the UAV-fixed body frame with respect to the LADAR. As a first approach, the average of all available measurements is considered, i.e.,

$$\mathbf{r}_{O_bL}^s = \frac{1}{N}\sum_{i=1}^{N}(\mathbf{r}_{iL}^s - \mathbf{T}_{sb}\mathbf{r}_{iO_b}^b) \tag{54}$$

Finally, the dynamics of the UAV can be recovered from

$$[x^o,\, y^o,\, h^o]^T = \mathbf{T}_{os}\mathbf{r}_{O_bL}^s + [X^o,\, Y^o,\, -Z^o]^T \tag{55}$$

where $\mathbf{T}_{os}$ is the rotation matrix from the LADAR to the inertial frame (assumed to be known) and

$$\phi = \mathrm{t}^{-1}\frac{T_{bo_{23}}}{T_{bo_{33}}}, \quad \theta = -\mathrm{s}^{-1}T_{bo_{13}}, \quad \psi = \mathrm{t}^{-1}\frac{T_{bo_{12}}}{T_{bo_{11}}} \tag{56}$$

where $\mathbf{T}_{bo} = \mathbf{T}_{bs}\mathbf{T}_{so}$ and $T_{bo_{ij}}$ denotes the ij-th component of the matrix $\mathbf{T}_{bo}$.

Since these estimations are made at a constant sampling frequency, they can be discretized at every time step t_k. Then, using a simple Euler discretization algorithm, the observation vector can be defined as

$$\boldsymbol{\eta}_k = [\dot{x}^o,\, \dot{y}^o,\, \dot{h}^o,\, \phi,\, \theta,\, \psi,\, \dot{\phi},\, \dot{\theta},\, \dot{\psi}]_k^T \tag{57}$$

which will be used for feedback purposes.

5.2. Landing Procedure

Given the stochastic nature of the landing pad motion and the presence of multiple uncertainties in the described system (e.g. wind, measurement noises, and model uncertainties), tracking an accurate landing trajectory is impracticable. For this reason, the landing trajectory is described by a straight line at the end of which the UAV can be recovered by a capture net.

5.3. Simulations

The feedback control law developed in the previous section is implemented here. Table 1 lists the physical parameters used in the simulations, which correspond to actual values of the Lambda Unmanned Research Vehicle [19] except for the inertia values. The saturation limits are assumed to be

$$|\,\delta_a\,| \leq 30^o, \quad |\,\delta_e\,| \leq 30^o, \quad |\,\delta_r\,| \leq 30^o, \quad 0 \leq \eta \leq 1$$

The initial conditions are taken as:

$$(y,\, h)_0 = (50,\, 25)\,\mathrm{m}, \quad V_0 = 26.14\,\mathrm{m/s}, \quad (\phi,\, \theta,\, \psi)_0 = (15^o,\, 3^o,\, -15^o)$$

The control objective is to track a trajectory defined by $(y,\, h)_d = (0,\, 0)$ and $V_d = 22.22$ m/s. Note that for this flight condition the trim angle of attack is $\alpha_0 = 7.11^o$.

The effectiveness of the controller (18) and (36) is demonstrated by applying it to the complete nonlinear system (1)-(6) and (7)-(8). The control parameters are chosen as $k_{\gamma_{2_a}} = 0.05$, $k_{\gamma_{3_a}} = 0.05$, $k_V = 0.5$, $\lambda_\phi = \lambda_\theta = \lambda_\psi = 3$, $\lambda_{\dot{\phi}} = \lambda_{\dot{\theta}} = \lambda_{\dot{\psi}} = 3$, $\mathbf{L} = \mathrm{diag}\{0.5,\, 0.5,\, 0.5\}$. Note that approximation (22) has been used for the "sign" function with $k = 10$ in (18) and (36). This approximation reduces the chattering

Table 1: Parameters for the Lambda UAV landing at sea level [19].

Parameter	**Value**	**Parameter**	**Value**
ρ	$1.225\,\mathrm{kg/m^3}$	g	$9.81\,\mathrm{m/s^2}$
m	$92.10\,\mathrm{kg}$	I_x	$83.75\,\mathrm{kg\cdot m^2}$
I_y	$137.43\,\mathrm{kg\cdot m^2}$	I_z	$210.99\,\mathrm{kg\cdot m^2}$
I_{xz}	$3.05\,\mathrm{kg\cdot m^2}$	S	$1.96\,\mathrm{m^2}$
b	$4.29\,\mathrm{m}$	c	$0.46\,\mathrm{m}$
C_{L_0}	0.7939	C_{L_α}	5.8200
C_{D_0}	0.0290	k_1	0
k_2	0.0363	C_{m_0}	0
C_{m_α}	-1.1010	$C_{m_{\delta_e}}$	-0.8449
C_{m_q}	-15.4000	C_{Y_β}	-0.4372
$C_{Y_{\delta_r}}$	0.2865	C_{Y_p}	-0.0016
C_{Y_r}	0.2601	C_{l_β}	-0.0145
$C_{l_{\delta_a}}$	0.2608	$C_{l_{\delta_r}}$	0.0022
C_{l_p}	-0.5538	C_{l_r}	0.0876
C_{n_β}	0.0600	$C_{n_{\delta_a}}$	-0.0137
$C_{n_{\delta_r}}$	-0.0943	C_{n_p}	-0.0360
C_{n_r}	-0.1650		

in the control inputs; however, some high frequency chattering is still expected due to the EKF implementation. This frequency can be further reduced by smoothening the output of the EKF algorithm. Noted that the control input signal is sent to the servos every 0.1 s.

The wind has been implemented using the "Dryden Wind Turbulence Model (Continuous)" MATLAB toolbox. In Fig. 2, a particular realization of a gust is shown for the Lambda Unmanned Research Vehicle flying at 15 m and 26.14 m/s. The wind speed at 6 m (W_{20}) is taken as 5 m/s. The mean wind speed is $V_{m_w} = 5$ m/s along the inertial lateral axis (i.e., $\psi_w = 0$).

The landing platform is assumed to be a barge with zero forward speed and a

heading angle of 135^o. Fig. 3 shows the barge motion for an irregular sea described by Modified Pierson-Moskowits spectrum with a significant wave height $h_{1/3} = 4$ m and dominant wave period $T = 7$ s.

A highly dense point cloud is typically expected to be obtained from the LADAR. For simulation purposes, $N = 38$ points have been considered and the cloud represented in Fig. 4. It has been assumed that UAV observations are made as far as 2000 m at a scan rate of 100 Hz (i.e., $\Delta t = 0.01$ s) with an accuracy of 15 cm (one standard deviation). These values reflects state of the art technologies (e.g. Leica LAS60 Airborne Laser Scanner).

Zero-mean process (gaussian) noises with standard deviation of 0.005 are assumed for the variables $[V_a,\ \gamma_{2_a},\ \gamma_{3_a},\ p_a^b,\ q_a^b,\ r_a^b]^T$. The following matrices were used for the estimation of the state variables:

$$\mathbf{Q} = 0.005^2\,\mathrm{diag}\{1,\ 1,\ 1,\ 0,\ 0,\ 0,\ 1,\ 1,\ 1\}$$

$$\mathbf{R} = 10(0.15)^2\,\mathrm{diag}\left\{\frac{10}{\Delta t},\ \frac{10}{\Delta t},\ \frac{10}{\Delta t},\ 1,\ 1,\ 1,\ \frac{1}{\Delta t},\ \frac{1}{\Delta t},\ \frac{1}{\Delta t}\right\}$$

As can be seen in Figs. 5-7, given the estimation (green line) of the inertial position and orientation of the UAV based on LADAR measurements, the EKF is applied (red line) and its estimation is used to obtain the control inputs. Given the deflection of the different control surfaces, the actual values (blue line) of the state variables are obtained. It can be seen that the velocity, lateral and vertical displacements as well as the Euler angles converge to the desired values for acceptable values of the control inputs.

Finally, the motion of the UAV relative to the barge is shown in Fig. 8 from which a net can be sized for recovery purposes.

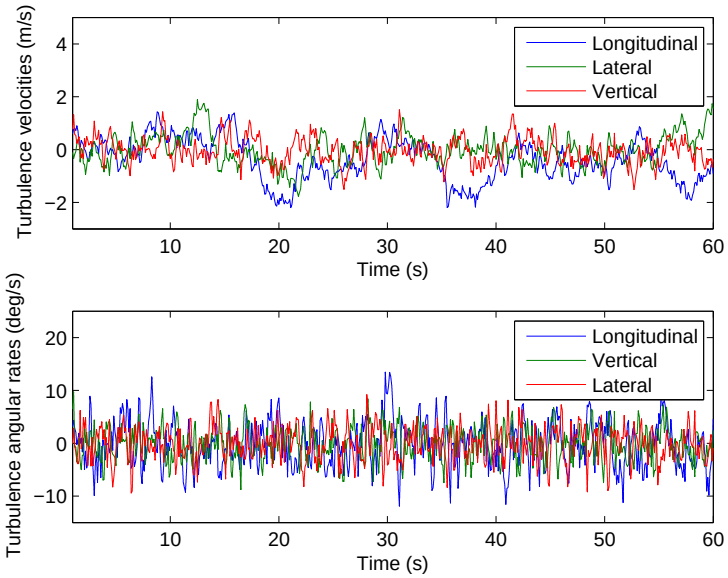

Figure 2: Turbulence velocities for the Lambda Unmanned Research Vehicle flying at 15 m and 26.14 m/s ($W_{20} = 5$ m/s).

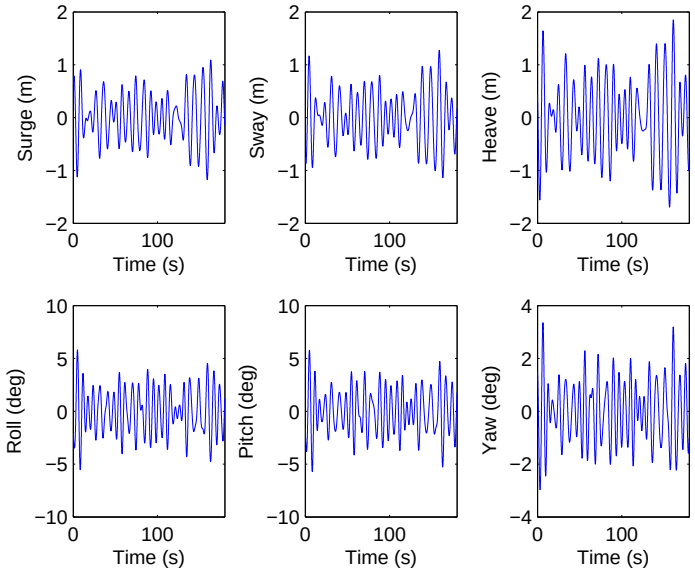

Figure 3: Surge, sway, heave, roll, pitch and yaw motions for a barge at 0 kts and heading angle of 135 deg (sea state described by Modified Pierson-Moskowits spectrum with $h_{1/3} = 4$ m and $T = 7$ s).

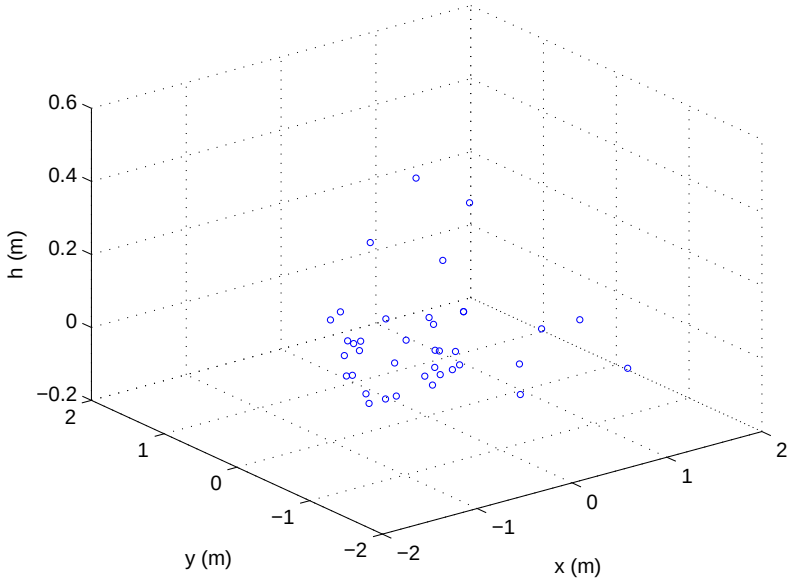

Figure 4: Cloud of points (centered at the UAV center of mass) observed by the LADAR.

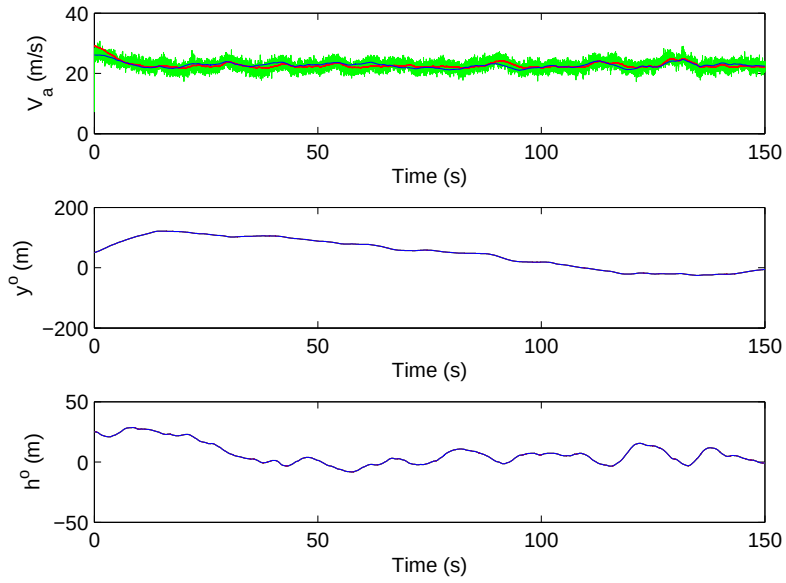

Figure 5: Time responses of the air velocity (V_a), inertial lateral displacement (y^o) and altitude (h^o) (blue line) compared with their estimate (green) and filtered (red) values.

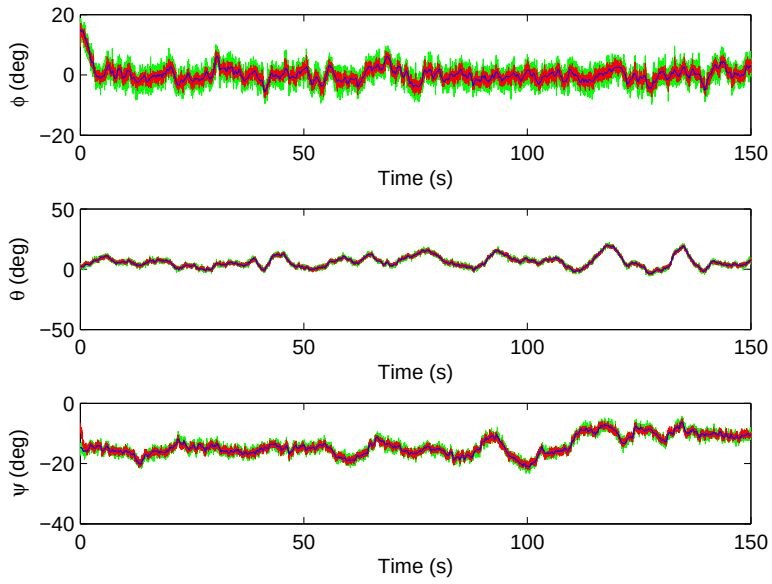

Figure 6: Time responses of the roll (ϕ), pitch (θ) and yaw (ψ) angles (blue line) compared with their estimate (green) and filtered (red) values.

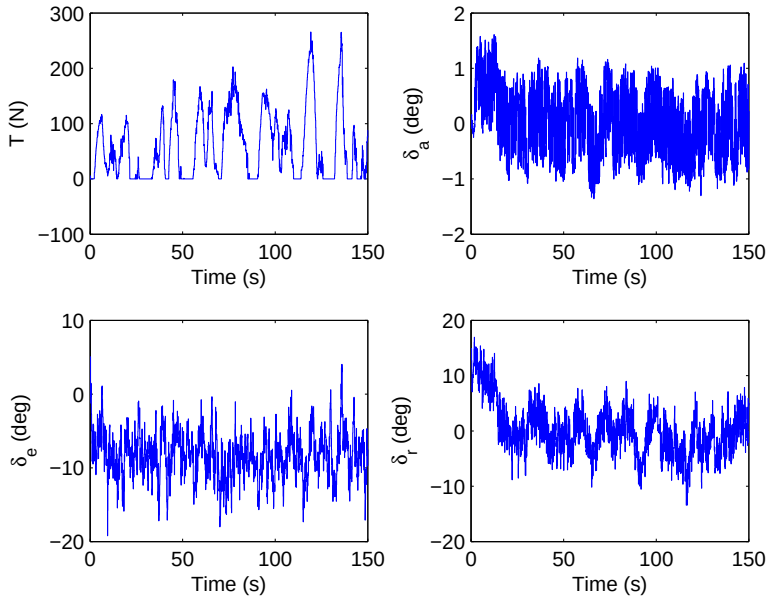

Figure 7: Time responses of the thrust (T), aileron (δ_a), elevator (δ_e) and rudder (δ_r) deflections.

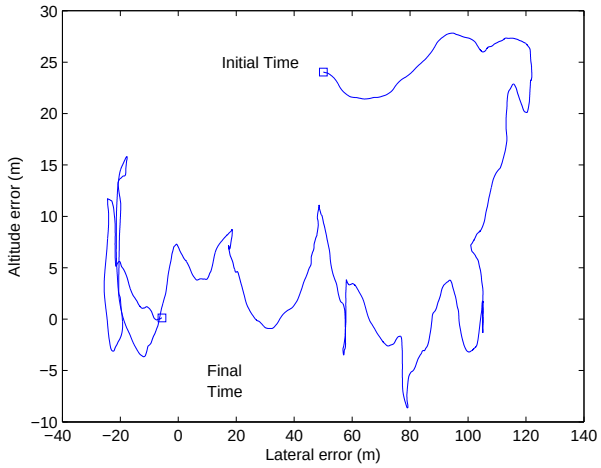

Figure 8: Relative motion of the UAV with respect to the barge.

6. Conclusion

A fully nonlinear aircraft dynamic model in the presence of wind has been introduced. A sliding mode controller has been designed to control the air velocity using the throttle position, and the rest of the dynamics via the aileron, elevator, and rudder deflections. The proposed controller has been shown to be applicable for highly nonlinear conditions including high angle of attack regime as well as being inherently robust to uncertainties and perturbations. An EKF method has been proposed for the state estimation and noise filtering. The applicability of the proposed controller has been illustrated through a case study: the landing control of a UAV on a ship deck in the presence of wind based exclusively on LADAR measurements. It has been shown that the full state converges to the desired values even in the presence of stochastic wind. Future research includes the implementation of the moving horizon estimation method for the state estimation problem. This optimization-based method treats both the state and parameter estimation within one problem, which also allows constraints to be incorporated.

Acknowledgment

The authors would like to thank the support provided by Nanyang Technological University.

Appendix A

Assuming the wind vortex hypothesis in [16], the wind is modeled by a local linear term around the aircraft and an angular velocity with respect to the Earth, such that:

$$\mathbf{V} = \mathbf{V}_a + \mathbf{V}_w, \quad \boldsymbol{\Omega} = \boldsymbol{\Omega}_a + \boldsymbol{\Omega}_w \tag{58}$$

where $\mathbf{V}$ and $\mathbf{V}_a$ denote the ground and the air velocity of the aircraft's center of mass, respectively; $\mathbf{V}_w$ is the wind velocity; and $\boldsymbol{\Omega}$, $\boldsymbol{\Omega}_a$, $\boldsymbol{\Omega}_w$ are the angular velocity of the aircraft relative to Earth, the aerodynamic angular velocity, and the local wind angular velocity relative to the Earth (atmospheric angular velocity relative to the Earth), respectively. Note that for the wind velocity, the definition above corresponds to the velocity of an atmospheric particle which could have been located at the center of mass of the aircraft.

Assuming the wind velocity can be split into its mean value and gust components, where the mean speed V_{m_w} acts in a horizontal plane at a heading angle ψ_w, the linear and angular velocity of the wind can be expressed in the body frame as follows:

$$\mathbf{V}_w^b = [u_w^b,\, v_w^b,\, w_w^b]^T = \mathbf{T}_{bo}[V_{m_w}\mathrm{s}\psi_w + u_{g_w}^o,\, V_{m_w}\mathrm{c}\psi_w + v_{g_w}^o,\, w_{g_w}^o]^T \tag{59}$$

and

$$\boldsymbol{\Omega}_w^b = [p_w^b,\, q_w^b,\, r_w^b]^T = \mathbf{T}_{bo}[p_w^o,\, q_w^o,\, r_w^o]^T \tag{60}$$

respectively, where

$$\mathbf{T}_{bo} = \begin{bmatrix} \mathrm{c}\theta\mathrm{c}\psi & \mathrm{c}\theta\mathrm{s}\psi & -\mathrm{s}\theta \\ \mathrm{s}\phi\mathrm{s}\theta\mathrm{c}\psi - \mathrm{c}\phi\mathrm{s}\psi & \mathrm{s}\phi\mathrm{s}\theta\mathrm{s}\psi + \mathrm{c}\phi\mathrm{c}\psi & \mathrm{s}\phi\mathrm{c}\theta \\ \mathrm{c}\phi\mathrm{s}\theta\mathrm{c}\psi + \mathrm{s}\phi\mathrm{s}\psi & \mathrm{c}\phi\mathrm{s}\theta\mathrm{s}\psi - \mathrm{s}\phi\mathrm{c}\psi & \mathrm{c}\phi\mathrm{c}\theta \end{bmatrix}$$

represents the transformation matrix from the inertial to the body frame.

The air velocity can be expressed in terms of the aerodynamic climb and track angles as follows:

$$\begin{bmatrix} u_a^b \\ v_a^b \\ w_a^b \end{bmatrix} = V_a \mathbf{T}_{bo} \begin{bmatrix} \mathrm{c}\gamma_{2_a}\mathrm{c}\gamma_{3_a} \\ \mathrm{c}\gamma_{2_a}\mathrm{s}\gamma_{3_a} \\ -\mathrm{s}\gamma_{2_a} \end{bmatrix} \tag{61}$$

For a truly symmetric configuration, standard expressions for the aerodynamic forces and moments can be written as follows:

$$L = QS\left(C_{L_0} + C_{L_\alpha}\alpha_a\right) \tag{62}$$

$$D = QS\left(C_{D_0} + k_1 C_L + k_2 C_L^2\right) \tag{63}$$

$$\mathcal{M} = QSc\left(C_{m_0} + C_{m_\alpha}\alpha_a + C_{m_{\delta_e}}\delta_e + \frac{c}{2V_a}C_{m_q}q_a^b\right) \tag{64}$$

$$Y = QS\left(C_{Y_\beta}\beta_a + C_{Y_{\delta_r}}\delta_r + \frac{b}{2V_a}(C_{Y_p}p_a^b + C_{Y_r}r_a^b)\right) \tag{65}$$

$$\mathcal{L} = QSb\left(C_{l_\beta}\beta_a + C_{l_{\delta_a}}\delta_a + C_{l_{\delta_r}}\delta_r + \frac{b}{2V_a}(C_{l_p}p_a^b + C_{l_r}r_a^b)\right) \tag{66}$$

$$\mathcal{N} = QSb\left(C_{n_\beta}\beta_a + C_{n_{\delta_a}}\delta_a + C_{n_{\delta_r}}\delta_r + \frac{b}{2V_a}(C_{n_p}p_a^b + C_{n_r}r_a^b)\right) \tag{67}$$

where $Q = \rho V_a^2/2$ is the dynamic pressure, ρ stands for the air density, S is the wing surface, c is the mean aerodynamic chord, and b is the wing span. The applicability of results of this paper can easily be extended to more general nonlinear mathematical models of the aerodynamic forces and moments.

References

[1] F. Gavilan, J. A. Acosta, R. Vazquez, Control of the longitudinal flight dynamics of an UAV using adaptive backstepping, in: Proceedings of the 18th IFAC World Congress, 2011.

[2] G. Chowdhary, E. Frazzoli, J. P. How, H. Lui, Handbook of unmanned aerial vehicles, Springer, 2012.

[3] F. Esfandiari and H. K. Khalil, Stability analysis of a continuous implementation of variable structure control, IEEE Transactions on Automatic Control 36 (5) (1991) 616-620.

[4] T. Espinoza, A. Dzul, M. Llama, Linear and nonlinear controllers applied to fixed-wing UAV, International Journal of Advanced Robotics Systems 10 (33) (2013) 1-10.

[5] H. C. Ferreira, R. S. Baptista, J. Y. Ishihara, G. A. Borges, Disturbance rejection in a fixed wing UAV using nonlinear H_∞ state feedback, in: Proceedings of IEEE International Conference on Control and Automation, 2011.

[6] W. MacKunis, Z. D. Wilcox, M. K. Kaiser, W. E. Dixon, Global adaptive output feedback tracking control of an unmanned aerial vehicle, IEEE Transactions on Control Systems Technology 18 (6) (2010) 1390-1397.

[7] Y. Rizwan, S. L. Waslander, C. Nielsen, Nonlinear aircraft modeling and controller design for target tracking, in: Proceedings of American Control Conference, 2011.

[8] Y. Kang and J. K. Hedrick, Linear tracking for a fixed-wing UAV using nonlinear model predictive control, IEEE Transactions on Control Systems Technology 17(5) (2009) 1202-1210.

[9] C. B. Low, A trajectory tracking control design for fixed-wing unmanned aerial vehicles, in: Proceedings of IEEE International Conference on Control Applications, 2010.

[10] J. Rubio Hervas, M. Reyhanoglu, H. Tang, Automatic landing control of unmanned aerial vehicles on moving platforms, in: Proceedings of IEEE International Symposium on Industrial Electronics, 2014.

[11] X. Yang, L. Mejias, T. Molloy, A gust-attenuation controller for fixed-wing UAVs during collision avoidance course, in: Proceedings of International Conference on Unmanned Aircraft Systems, 2012.

[12] C. Liu, O. McAree, W. H. Chen, Path-following control for small fixed-wing unmanned aerial vehicles under wind disturbances, International Journal of Robust and Nonlinear Control 23 (2013) 1682-1698.

[13] A. Brezoescu, T. Espinoza, P. Castillo, R.. Lozano, Adaptive trajectory following for a fixed-wing UAV in presence of crosswind, Journal of Intelligent & Robotic Systems 69 (2013) 257-271.

[14] A. Brezoescu, P. Castillo, R. Lozano, Wind estimation for accurate airplane path following applications, in: Proceedings of International Conference on Unmanned Aircraft Systems, 2013.

[15] S. Mills, N. Aouf, L. Mejias, Image based visual servo control for fixed wing UAVs tracking linear infrastructure in wind, in: Proceedings of IEEE International Conference on Robotics and Automation, 2013.

[16] J. L. Boiffier, The dynamics of flight: equations, John Wiley & Sons, 1998.

[17] J. Rubio Hervas, M. Reyhanoglu, H. Tang, Nonlinear automatic landing control of unmanned aerial vehicles on moving platforms via a 3D laser radar, in: Proceedings ICNPAA World Congress: Mathematical Problems in Engineering, Sciences and Aerospace, 2014.

[18] J. R. Wertz, Spacecraft attitude determination and control, Kluwer Academic Publishers, 1978.

[19] G. A. Swift, Model identification and control design for the Lambda Unmanned Research Vehicle, Master's Thesis, Air Force Institute of Technology, WPAFB OH 45433-6583, 1991.